European Journal of Pharmaceutics and Biopharmaceutics 197 (2024) 114238

Contents lists available at ScienceDirect

European Journal of Pharmaceutics and Biopharmaceutics

journal homepage: www.elsevier.com/locate/ejpb

Development of cationic solid lipid nanoparticles incorporating cholesteryl-9-carboxynonanoate (9CCN) for delivery of antagomiRs to macrophages

Adrian Mallén [a], David A. Narváez-Narváez [c], M.D. Pujol [e], Estanis Navarro [a], Josep Maria Suñé-Negre [c,d], Encarna García-Montoya [c,d], Pilar Pérez-Lozano [c,d], Benjamín Torrejón-Escribano [f], Marc Suñé-Pou [c,d,*,1], Miguel Hueso [a,b,*,1]

[a] Experimental Nephrology Lab, Institut d'Investigació Biomèdica de Bellvitge-IDIBELL, L'Hospitalet de Llobregat, Spain
[b] Department of Nephrology, Hospital Universitari Bellvitge, and Institut d'Investigació Biomèdica de Bellvitge-IDIBELL, L'Hospitalet de Llobregat, Spain
[c] Service of Development of Medicines (SDM), Faculty of Pharmacy, University of Barcelona, Barcelona, Spain
[d] Pharmacotherapy, Pharmacogenetics and Pharmaceutical Technology Research Group, Bellvitge Biomedical Research Institute (IDIBELL), Barcelona, Spain
[e] Service of Pharmacology, Toxicology and Therapeutic Chemistry, Faculty of Pharmacy, University of Barcelona, Barcelona, Spain
[f] Advanced Light Microscopy Unit (Bellvitge Campus), Scientific and Technical Facility (CCiTUB), University of Barcelona, L'Hospitalet de LLobregat, Spain

ARTICLE INFO

Keywords:
Solid lipid nanoparticles (SLNs)
AntagomiR-125b
Macrophage transfection
Nucleic acid delivery
miR-125b
Cholesteryl-9-carboxynonanoate (9CCN)

ABSTRACT

Lipid-based nanoparticles are a useful tool for nucleic acids delivery and have been regarded as a promising approach for diverse diseases. However, off-targets effects are a matter of concern and some strategies to improve selectivity of solid lipid nanoparticles (SLNs) were reported. The goal of this study was to test formulations of SLNs incorporating lipid cholesteryl-9-carboxynonanoate (9CCN) as "eat-me" signal to target antagomiR oligonucleotides to macrophages. We formulate four SLNs, and those with a mean diameter of 200 nm and a Z-potential values between 25 and 40 mV, which allowed the antagomiR binding, were selected for in vitro studies. Cell viability, transfection efficiency and cellular uptake assays were performed within in vitro macrophages using flow cytometry and confocal imaging and the SLNs incorporating 25 mg of 9CCN proved to be the best formulation. Subsequently, we used a labeled antagomiR to study tissue distribution in in-vivo ApoE-/- model of atherosclerosis. Using the ApoE-/- model we demonstrated that SLNs with phagocytic signal 9-CCN target macrophages and release the antagomiR cargo in a selective way.

1. Introduction

Nucleic acid release and gene silencing are currently promising therapeutic tools, although the control of their effectivity, correct "in vivo" delivery and possible off-target effects, due to lack of selectivity, remains challenging [1]. In this context, several small non-coding RNAs like small interfering RNAs (siRNA), micro RNAs (miRNAs), piwi-interacting RNAs (piRNAs) and small nuclear RNAs (snRNAs) have been used for in vivo delivery [2]. The small non-coding microRNAs (miRNAs), which modulate gene expression at the post-transcriptional level by targeting the 3'UTR of mRNA ([3]; see also Navarro et al [4] for a recent review), play a critical role in pathological diseases since they have multiple targets and their activity differs depending on the cell type where they are expressed; therefore, their potential to be used as biomarkers or therapeutic targets have been increasing in the last few years [1,5,6]. For this reason, the expression control of endogenous miRNAs mediated by antagomiRs, chemically modified oligonucleotides that bind specifically to a particular miRNA, have developed an important role as emerging therapeutic tools for diverse diseases [7,8]. Despite this, many limitations in the delivery of "naked" nucleic acid have been described due to the intrinsic instability of the molecules, off-target effects, degradation by endonucleases and the low specificity for

* Corresponding authors at: Service of Development of Medicines (SDM), Faculty of Pharmacy, University of Barcelona, Barcelona, Spain (M. Suñé-Pou). Department of Nephrology, Hospital Universitari Bellvitge, and Institut d'Investigació Biomèdica de Bellvitge-IDIBELL, L'Hospitalet de Llobregat, Spain (M. Hueso).
E-mail addresses: amallen@idibell.cat (A. Mallén), mdpujol@ub.edu (M.D. Pujol), jmsune@ub.edu (J. Maria Suñé-Negre), torrejonbenja@ub.edu (B. Torrejón-Escribano), marcsune@ub.edu (M. Suñé-Pou), mhueso@idibell.cat (M. Hueso).
[1] MSP and MH contribute equally.

https://doi.org/10.1016/j.ejpb.2024.114238
Received 27 October 2023; Received in revised form 22 February 2024; Accepted 25 February 2024
Available online 27 February 2024

their targets. Alternatively to chemical modification in therapeutic oligonucleotides [9], the development of a nucleic acid encapsulation and delivery system based on nanoparticles (NPs) is one of the main fields in current nanotechnology since its therapeutic effects have been demonstrated in a large number of in vivo assays and clinical trials [10–12].

Nanoparticle carriers offer controlled delivery of nucleic acids, thus improving transport efficiency and distribution among tissues and limiting adverse effects [13,14]. However, the in vivo fate of nucleic acid-loaded NPs, their tissue and cell targeting and accessibility in organs with continuous capillaries, and their encapsulation efficiency are still limited and remain challenging [15,16]. The addition of specific ligand molecules in NPs and modifications of the chemical structures or physicochemical properties are useful strategies for manipulating the fate of NPs in vivo, as demonstrated by Zhang et al [17]. It is also known that introducing positively charged molecules, like cationic lipids, prior to the emulsification process have facilitated the delivery of in vivo therapeutic RNAs [18,19]. Particularly, lipid-based nanoparticles (LNPs) composed of a lipid bilayer with aqueous core can efficiently encapsulate or bind miRNAs by spontaneous electrostatic interactions between cationic lipids and negatively charged RNA molecules, making the RNA extremely stable and protected from RNases when compared to in vivo administered naked RNAs [20,21]. However, the use of cationic lipids is commonly associated with cell toxicity, as they can disrupt cell membrane integrity, induce cytoplasmic vacuolization and reduce cell activity, apart from forming aggregates due to the interaction with negatively charged serum proteins [22,23]. Thus, several strategies to reduce the cationic charge have been attempted. The use of cholesteryl oleate in cationic solid lipid nanoparticles (SLNs) formulations have been demonstrated to improve cytotoxicity and nucleic acid delivery [24,25]. Suñé-Pou et al [23] concretely showed mechanisms by which cationic SLNs increased DNA and RNA transfection efficiency.

It is clear that after the administration of nucleic acids encapsulated with LNPs, the cargo is rapidly accumulated in the liver due to the substantial flow rate, and to the clarification of NPs via Kupfer cells [16]. The developing of extrahepatic targeting has become another challenge for the treatment of atherosclerosis diseases based on NPs delivery system. Aortic macrophages from the intima play a crucial role in the pathophysiology and development of atheroma plaques and several miRNAs have been implicated in the process [26]. In concrete, our group found that miR-125b is a pathogenic player in vascular diseases whose expression is up-regulated in macrophages from coronary artery diseases, valve calcification and atheroma plaques from ApoE-/- mice [27–29]. In this context of the need to incorporate some ligand to target the anti-miRNA-loaded NPs, recent studies have found that “eat-me” signal lipids like phosphatidylserine (PtdSer) and cholesteryl-9-carboxynonanoate (9CCN), present in the membrane of apoptotic cells, allows them to be recognized by the macrophages present in atherosclerotic plaques, so that these signals can be incorporated in nanoparticles and be used for targeting and imaging macrophages [30–32]. Since PtdSer is a highly anionic lipid that can interfere in lipoplex formation between the NP and the antagomiR, we favored the use of the 9-CCN, a common oxidized lipid present in both intracellularly and extracellularly macrophages from advanced atherosclerotic lesions, as the optimal candidate for in vivo macrophage targeting [32]. Moreover, Bagalkot et al [33] reported that lipid-latex (LiLa) NPs incorporating the phagocytic signal 9-CCN, were selectively deposited to M1 macrophages in a mouse model of atherosclerosis. In vivo MRI imaging using 9-CCN- NPs revealed colocalization of these vesicles with arterial macrophages which were not seen in control vesicles without 9-CCN. Nanoparticles containing 9-CCN also demonstrated a prolonged plasma and plaque retention in a rabbit model of atherosclerosis as reported by Maiseyeu et al [32].

In the present study we have designed a modified version of cationic solid lipid nanoparticles containing a 9-CCN “eat-me” phagocytic signal for the specific targeting of macrophages, as represented in the schematic illustration of chemical structures components and SLN interaction with macrophages from Fig. 1Our aim was improving the delivery and arrival of an anti-miR-125b antagomir to target cells in vivo greatly reducing off-target effects. Thus, four vesicle formulations of SLNs were prepared using the hot microemulsification method described by Fàbregas et al [34], and the lipid matrix was varied according to the concentrations of 9CCN. In vitro and in vivo evaluation of these nanoparticles was carried out and compared with control naked antagomiR molecules, which lack a lipid vesicle protection that drives them to RNase degradation and later elimination by the liver without reaching its fate in vivo. SLNs with modified cholesterol lipid 9-CCNs are easily fabricated in the laboratory, and allow improved recognition and subsequent uptake by macrophages, making them a promising in vivo antagomiR delivery technology.

2. Material and methods

2.1. Animals

Experiments were performed in 10-week-old ApoE-/- mice on C57BL/6 background (3 males and 3 females; Jackson Laboratories, Bar Harbor, ME, USA) fed with a “high fat rodent diet” ad libitum that contained 1.25 % cholesterol and provided 40 % of the energy as fat (D12108CI; Research Diets Inc, New Brunswick, NJ, USA) for 20 weeks. Mice were randomized into an 9CCN-25 mg + Cy5_antagomiR-125b SLN group (n = 3; 15 mg/kg, 1 dose) and a control group treated with naked Cy5_antagomiR-125b (n = 3; 15 mg/kg, 1 dose). For SLNs group, the Cy5_antagomiR-125b was resuspended in PBS, mixed with filtered (43–46 μm filters) 9CCN-25 mg SLNs (45 % of total volume), and incubated for 30 min at RT until the SLNplexes were formed. Dose was chosen from previous experiments not published (Data not shown). These were subsequently administered subcutaneously to mice. After 24 h of administration, animals were euthanized at 30 weeks of age by the inhalation of < 5 % isoflurane (PDG96236, Baxter Corporation, IL, USA) and cardiac puncture in order to observe the arrival of fluorescence Cy5-loaded antagomiR-125b to different tissues. Serum was also collected at the end of the study and total Urea, ALT, AST and Creatinine parameters were measured at the Clinical Veterinary Biochemistry Service of the Universitat Autónoma of Barcelona (UAB). The Cy5-loaded antagomiR-125b (in vivo HPLC formulation; CTM-676490) was developed by Dharmacon (Colorado, USA) and the sequence was as follows: 5’Cy5.mU.*.mC.*.mA.mC.mA.mA.mG.mU.mU.mA.mG.mG.mG.mU.mC.mU.mC.mA.mG.*.m G.*.mG.*.mA.*0.3’-Chl 3’. All animal studies were carried out in accordance with recommendations in the Guide for the care and use of Laboratory Animals of the National Institutes of Health. The protocol was approved by the Committee on the Ethics of Animal Experiments of UB-Bellvitge (number 85/20).

2.2. Synthesis of 9-CCN

1 g cholesterol plus 1.4 g azelaic acid, 1.9 g N-(3-dimethylaminopropyl)-N’-ethylcarbodiimide hydrochloride and 610 mg 4-(dimethylamino) pyridine were mixed in 20 mL of 1:1 acetone-chloroform and flushed with nitrogen (reagents purchased from Sigma-Aldrich, St Louis, MO, USA). The mixture was vigorously stirred overnight, concentrated and purified by column chromatography on silica gel by using dichloromethane-methanol mixture as the eluent (9:1 by volume) to give 9-CCN as a colorless solid. The purity of 9CCN was assessed by NMR as shown in Figure S3 from Supplementary Information. 9CCN fabrications were performed in the Service of Pharmacology, Toxicology and Therapeutic Chemistry from Universitat de Barcelona by Dr Pujol.

2.3. Production of Solid Lipid Nanoparticles (SLNs)

SLNs were synthesized using the hot microemulsification method [35]. Briefly, a lipid matrix containing stearic acid (K4656336152, EMD Millipore, Billerica, USA) and cholesteryl oleate (L7EJD-E0, Tokyo

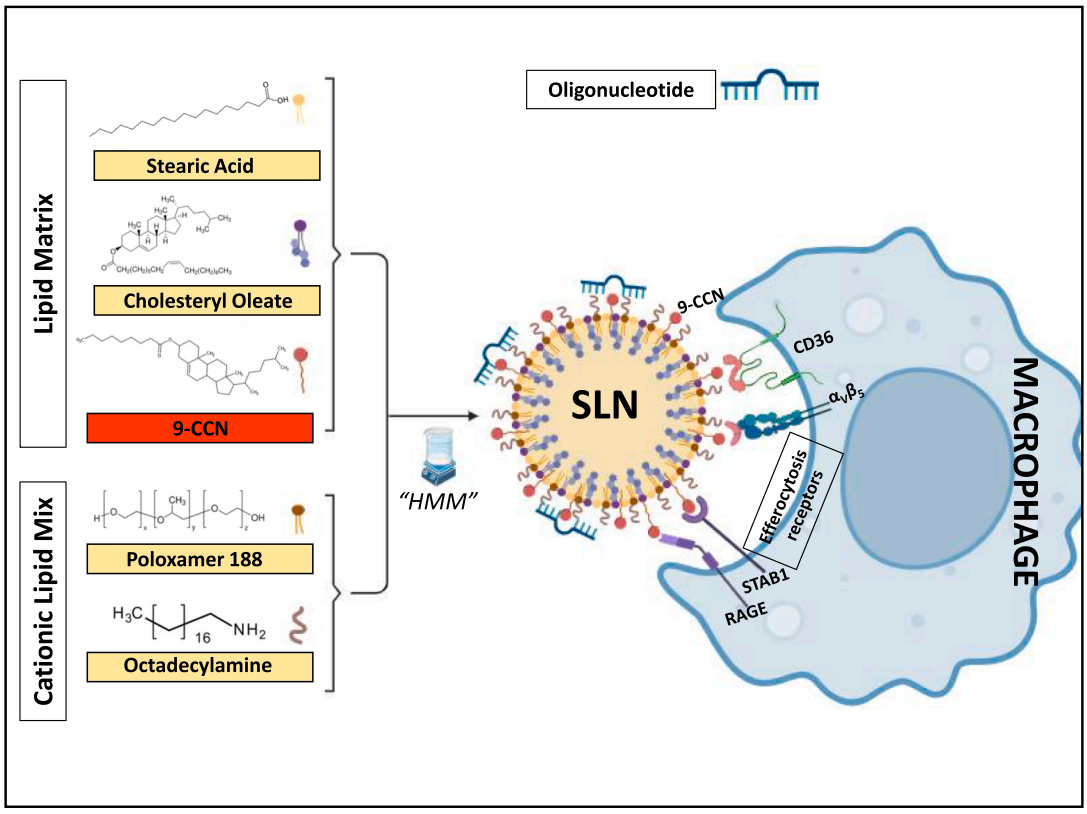

Fig. 1. Schematic illustration of 9-CCN SLNs components and its biological interaction with macrophages. Chemical structures of all the components used for the synthesis of SLNs are presented in the left side of the image. Stearic acid (yellow lipid), cholesteryl oleate (purple lipid), and 9-CCN (red lipid) were used for the lipid matrix of the nanoparticles and were mixed with poloxamer 188 (brown lipid) and octadecylamine (brown curved molecule) of the cationic lipid mix. After the hot microemulsification method described below, SLNs were synthetized. The SLNplex were formed by mixing SLNs with the appropriate oligonucleotide (e.g.: anti-miR125b). The targeting to macrophages was achieved by the phagocytic "eat-me" signal of cholesterol-9-carboxynonanoate (9-CCN), which is biologically externalized in the membrane of apoptotic cells. Macrophages interact with 9-CCN either directly with phagocytic receptors (e.g.; STAB1, RAGE) or indirectly through bridging molecules (e.g.; TSP1 with CD36, CYR61 with $\alpha_V\beta_5$) as reported in the right side of the image. **Abbreviations**: 9CCN, cholesteryl-9-carboxynonanoate; SLNs, Solid Lipid Nanoparticles, STAB1, Stabilin-1; RAGE, Receptor for advanced glycation endproducts; TSP1, Thrombospondin-1; CD36, cluster of differentiation 36; CYR61, cysteine-rich angiogenic protein 61; $\alpha_V\beta_5$, Integrin alpha-v beta-5. (For interpretation of the references to colour in this figure legend, the reader is referred to the web version of this article.)

Chemical Industry TCI, Zwijndrecht, Belgium) were poured onto a cationic lipid mix composed by poloxamer 188 (SLBF9298V, Sigma-Aldrich, St Louis, MO, USA), octadecylamine (A0307242, Acros Organics, Geel, Belgium) and ultrapure water in order to form a hot emulsion. All previous components were heated between 5 and 10 °C above their melting points (near to 80 °C) and stirred for 10 min. The microemulsion was dispersed with continuous agitation using refrigerated water (4 °C) for core solidification and centrifuged at 19.000*g* for 15 min and double filtered using qualitative filters of 43–48 μm and 7–9 μm. Different concentrations of 9CCN were incorporated to the lipid matrix (Table 1) to confer the SLNs a "eat-me" signal lipid. These SLNs were lyophilized (L-3 Telstar, Terrassa, Spain) using trehalose (5 % w/v 1:1) as a cryoprotectant to improve their stability and to preserve their properties. For lyophilization process, a freezing cycle of 4 h at −55 °C was performed, followed by a primary drying of 0.100 mbar of vacuum and −15 °C for 72 h, and a secondary drying at 25 °C for 24 h.

2.4. Determination of SLN particle size and surface charge

Particle size was determined by laser diffractometry on a Mastersizer 2000 (Malvern Instruments, UK) in triplicate, by using appropriate amounts of sample until correct obscuration percentage was achieved. Particle size in nanometers (nm) was determined by applying a Fourier transform to measured diffracted angles via Zetasizer software.The surface potential (Z potential) and polydispersity index (PDI) were also measured using laser Doppler micro-electrophoresis and electrophoretic light scattering in Zetasizer Nano-Z (Malvern Instruments, UK). Briefly, a cell containing the sample was connected to electrodes and electrophoretic mobility was converted to Z potential expressed in millivolts (mV) using specialized Zetasizer software. All analyses were performed in triplicate and average and standard deviation are recorded in Table S1.

2.5. TEM morphological analysis

Surface of the SLNs was analyzed by Transmission Electron Microscopy (TEM). First, lyophilized nanoparticles were reconstituted with 6 mL of purified water and filtered with 43–48 μm filters, placed in an UV-activated 200Mesh carbon-coated copper grid (930342, Sigma-Aldrich, St Louis, MO, USA), negatively stained with 4 % uranyl acetate solution with methylcellulose, dried and placed in a Petri dish for image acquisition. Images were acquired with Tecnai Spirit microscope (FEI Company, Hillsboro, OR, USA) equipped with Lab8 cathode and Megaview camera at 120 kV.

2.6. Stability assay

Stability of lyophilized SLNs was checked during 48 weeks by analyzing the particle size, Z potential and PDI after nanoparticle reconstitution with 6 mL of purified water and filtration with 43–46 μm

Table 1
Composition of the different solid lipid nanoparticles formulations and characteristics of freshly fabricated SLNs from each formulation Diameter, Z-potential and Poli-dispersion index data are expressed as mean ± SD (n=3 independent quantifications). *Abbreviations: 9-CCN, cholesteryl-9-carboxynonanoate; PDI, poli-dispersion index; NE, non-evaluated; SD, Standard deviation.*

Components	**SLNs 9CCN-150 mg**	**SLNs 9CCN-100 mg**	**SLNs 9CCN-50 mg**	**SLNs 9CCN-25 mg**	**SLNs Ctrl**
Stearic acid (mg)	140	160	180	190	200
Cholesteryl oleate (mg)	210	240	270	285	300
9CCN (mg)	150	100	50	25	–
Octadecylamine (mg)	600	600	600	600	600
Poloxamer 188 (mg)	100	100	100	100	100
Characteristics of fresh SLNs	**SLNs 9CCN-150 mg**	**SLNs 9CCN-100 mg**	**SLNs 9CCN-50 mg**	**SLNs 9CCN-25 mg**	**SLNs Ctrl**
Diameter (nm)	341.9 ± 11.12	651.4 ± 492.6	244.2 ± 4.26	212.5 ± 1.55	254 ± 2.31
Z-potential (mV)	36.7 ± 0.90	34 ± 2.39	37.6 ± 0.12	34 ± 0.75	35.3 ± 0.40
Poli-dispersion index (PDI)	0.285 ± 0.038	0.758 ± 0.223	0.124 ± 0.040	0.125 ± 0.010	0.085 ± 0.036
Binding capacity limit (ng)	NE	NE	1000	2000	2000

filters. Lyophilized vials of control SLNs, 9CCN-25 mg SLNs, 9CCN-50 mg SLNs, 9CCN-100 mg SLNs and 9CCN-150 mg SLNs were stored at 4 °C or 25 °C for 1, 4, 8, 24, 36 and 48 weeks until stability verification. Each analysis was performed in triplicate in Zetasizer Nano-Z (Malvern Instruments, UK). Raw data, average and standard deviation from each analysis are shown in a complete table in Supplementary Information Table S2. The stability assay complete graphs can be made available on demand, as they would take up too much space.

2.7. SLNplex formation in agarose gel and UV–VIS spectrophotometry

Binding capacity and loading efficiency of synthesized SLNs were determined by the incorporation of plasmidic DNA to SLNs (SLNplex). The SLNplex were prepared by adding different concentrations (500 ng, 1000 ng, 2000 ng, 3000 ng) of pmirGLO luciferase plasmid (E1330, Promega, Madison, WI, USA) to 15 μL of each formulation of SLNs: Control, 9CCN-25 mg or 9CCN-50 mg. The mixture was kept at RT for 30 min to allow the complexes to form. The SLNs:DNA lipoplexes, free SLNs and free plasmidic DNA were loaded on a 0,8% agarose electrophoresis gel containing 0.01 μg/mL SybrSafe (S33102, Thermofisher, Waltham, MA, USA) for nucleic acid visualization at 89 V for 35 min in a GelDoc XR system (BioRad, Hercules, CA, USA) with BioRadImageLab 5.2.2 software. The plasmidic DNA (500 ng/uL) and 9CCN-25 mg SLNs (1:2 dilution in purified H_2O) were used alone or combined in a SLNplex for obtaining the UV–VIS spectrophotometry spectrum in a Cary UV–VIS Multicell Peltier system (Agilent Technologies, California, USA).

2.8. Cell culture and cell viability assay

Cell viability was assessed with HEK293ft cells (2x10^5 cell/mL) grown in a 6-well plates (Thermofisher, Waltham, MA, USA) in Dulbecco's modified Eagle medium (DMEM) (11965092, Gibco-Thermofisher, Waltham, MA, USA). Different volumes of each filtered and lyophilized SLN formulations, in the range of 5–25 μL, were added to confluent HEK293ft cells and processed for cytotoxicity assays with 20 μg/mL Propidium Iodide (P1304MP, Thermofisher, Waltham, MA, USA). Viability was assessed with a BD FACS Canto flow cytometer (BD Biosciences, San Jose, CA, USA) by quantifying the % of PI-positive cells at 617 nm.

2.9. In vitro transfection assays

RAW264.7 murine macrophage cells (2×10^5) were grown in 6-well plates (Thermofisher, Waltham, MA, USA) with Dulbecco's modified Eagle medium (DMEM) supplemented with 10 % FBS, 1 % L-Glutamine and 1 % Penicillin/Streptomycin (P/S) until they reached 80 % confluence. SLNplexes were formed by mixing 12 μL of SLNs (9CCN-25 mg, 9CCN-50 mg or Control) with 60 nM of Cy-5-labelled antagomiR-125b (CTM-676490, Dharmacon, Lafayette, CO, USA) in 1 mL non-supplemented DMEM, leaving at RT for 30 min to allow the complexes to form. The complexes were added to every well and after 8 h the medium was supplemented with 10 % FBS, 1 % L-Glutamine and 1 % P/S. As a transfection control, 60 nM Cy5-antagomiR-125b were transfected into the cells using TransIT-X2 (#6004 MirusBio, Wisconsin, USA) according to manufacturer's protocol. After 48 h post-transfection cells were harvested and prepared for transfection efficiency analysis by flow cytometry in a BD FACS Canto cytometer using the cutoff values obtained from unstained RAW264.7 cells to subtract the auto-fluorescence signal of the cells. The Cy5-FITC fluorescence at 488/525 nm channel was used to determine the percentage of transfection as analyzed by the BD FACS Diva™ v9.0 Software (BD Biosciences, San Jose, CA, USA).

2.10. RNA isolation and RT-qPCR

Total RNA from tissues or cells were isolated using TRIzol reagent (15596026, Invitrogen, Carlsbad, CA, USA) according to the manufacturer's protocol. cDNA was generated using TaqMan reverse transcription kit Assay (4366596, Applied Biosystems, Foster City, CA, USA) for miRNA and was subjected to quantitative Real-Time PCR amplification using the TaqMan Universal qPCR Master Mix (4304437, Applied Biosystems, Foster City, CA, USA). Specific TaqMan probes (Applied Biosystems, Foster City, CA, USA) were used for hsa-miR-125b (Assay ID: 000449, Cat. Num.: 4427975 ThermoFisher Scientifics, Waltham, MA, USA) and U6 snRNA (Assay ID: 001973, Cat. Num.: 4427975 ThermoFisher Scientifics, Waltham, MA, USA) as internal control gene. Reactions were run on a Quantstudio System (AppliedBiosystems, Foster City, CA, USA). The relative miRNA expression levels were calculated using the ΔΔCt method.

2.11. Confocal imaging

At the time of mice sacrifice; liver, skin, heart and kidneys were removed, and fixed in 4 % paraformaldehyde with cold PBS for 12 h. These were further washed with PBS, rinsed overnight in PBS containing 30 % sucrose and mounted in OCT medium. Tissue blocks were cut into serial 10 μm-thick sections, dried 15 min at RT, embedded with DAPI mounting medium (NC9293783 SantaCruz Biotechnology, Dallas TX USA) and covered with a glass coverslip keeping the slides at 4 °C dark until microscope imaging. For aortic valves visualization, heart blocks were cut until they reached into the same anatomic location (170 mm after the appearance of the 3rd valve). Imaging was performed using a Carl Zeiss LSM880 spectral confocal microscope equipped with a 63 X objective 641 nm laser was used to excite the Cy5-antagomiR-125bwhile a 405 nm laser was used for for DAPI. Images were analyzed with Zen 2.3 SP1 (Black) v14.0 Software (Zeiss, Oberkochen, Germany). The relative number of positive anti-miR125b Cy5 marked cells was calculated by counting the positive cells with the ImageJ v1.53 (Maryland, USA) inside 3 separated areas (corresponding to a total of 100 cells per area) within the aortic lesion of the same section and the mean average of 3 areas was normalized by total number of cells in each mouse.

2.12. Statistical analyses

Statistical analyses were performed using the R package, version 4.1.3 (2022-03-10) and graphics with GraphPad Prism 8.0 for Windows (GraphPad Software Inc, CA, USA) with 2-tailed paired student T-test to describe significance variance between groups. Mean data was presented with ±SD, and P-values were represented by asterisks (* $P < 0.05$; **$P = 0.01–0.001$; *** $P < 0.001$).

3. Results

3.1. Fabrication and characterization of SLNs

Hot microemulsification technique was used for the fabrications of different formulations of SLNs in order to obtain small and not very polydisperse NPs preparations around 200 nm. Using a stable quantity of cation lipid mix used for the main structure of the NPs, the lipid matrix proportions of SLNs were changed according to the amount of 9CCN added (Table 1). As demonstrated by Suñé-Pou et al. (2018), to ensure stable SLNs with good diameter, PDI and Z-potential, it is necessary to maintain the ratios of Cholesteryl oleate, Stearic acid, Poloxamer and Octadecylamine as the "Ctrl SLNs" in Table 1. For this reason, we started by adding the lipid 9CCN at small amounts with respect to the total lipid matrix, being the ratio of 9CCN 5 % for SLNs + 25 mg 9CCN, 10 % for SLNs + 50 mg 9CCN, 20 % for SLNs + 100 mg 9CCN and 30 % for SLNs + 25 mg 9CCN. Due to the instability and complexity of the freshly prepared SLNs suspensions, the NPs with appropriate size (150–250 nm), Z-potential (+25–45 mV) and PDI (<0.2) were selected for the lyophilization process.

After lyophilization, resuspension in 6 mL of H_2O nuclease-free and filtration with 43–45 μm filters, previous parameters were re-analyzed and we observed that the diameters of SLNs formulation 9CCN-25 mg (212.5 nm) and 9CCN-50 mg (244.2 nm) were the size that we expected compared with SLNs Ctrl (254 nm), while the average diameters of SLNs formulations 9CCN-100 mg (651.4 nm) and 9CCN-150 mg (341.9 nm) were bigger (Table 1). Dispersion of nanoparticle populations was also evaluated and PDIs of 0.085, 0.125 and 0.124 were determined for SLN Ctrl, 9CCN-25 mg and 9CCN-50 mg formulations respectively, while PDIs of 0.758 and of 0.285 were found for 9CCN-100 mg and 9CCN-150 mg respectively, suggesting that both formulations with higher concentration of 9CCN developed more disperse populations of NPs and the presence of more aggregates. The difference between the diameter of SLNs + 100 mg and 150 mg 9CCN is due to the fact that in the case of SLNs + 100 mg 9CCN, the occurrence of a second nanoparticle population peak makes the mean diameter more biased and the mean diameter higher as well as the dispersion index. Z-potentials were also analyzed and all the formulations exhibit enough positive surface suitable for sufficient nucleic acid binding: 9CCN-Ctrl (35.3 mV), 9CCN-25 mg (34 mV), 9CCN-50 mg (37.6 mV), 9CCN-100 mg (34 mV), and 9CCN-150 mg (36.7 mV).

After lyophilization, stabilization assays for each formulation were made at25 °C as recommended by the ICH guidelines for long-term and accelerated storage of nanoparticles but they were also made at 4 °C to observe if there were differences at low temperatures. Particle diameter, Z-potential and PDI were assessed in this assay. during 48 weeks. The SLNs Ctrl, 9CCN-25 mg and 9CCN-50 mg formulations showed not major alterations regarding size, PDI and surface charge in both 4 °C or 25 °C conditions, suggesting that lyophilized powder SLNs can be used within 48 weeks of its fabrication. Conversely, 9CCN-100 mg and 9CCN-150 mg formulations exhibited disproportionate NPs size and inappropriate PDI

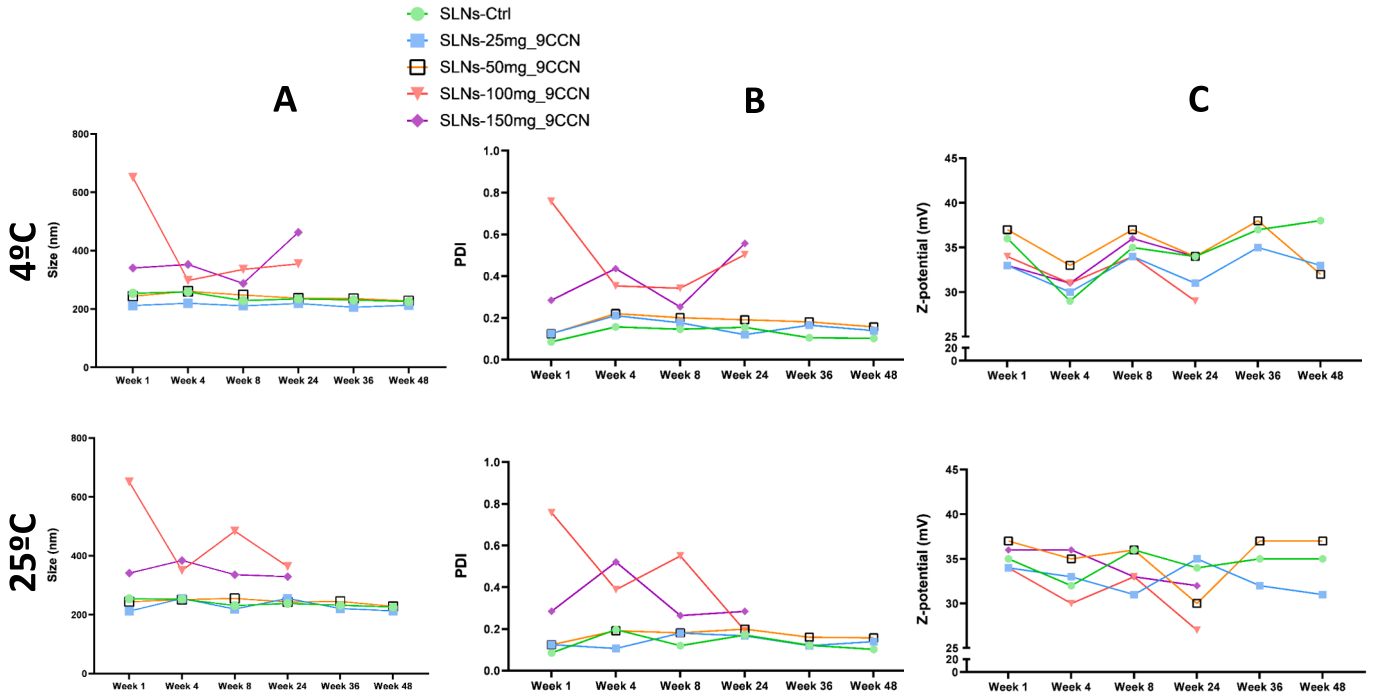

Fig. 2. Stability assay of lyophilized SLNs formulations during 48 weeks incubated at 4 °C (upper side) and at 25 °C (lower side). SLNs Ctrl are shown in green dots, SLNs + 25 mg of 9CCN are shown in blue squares, SLNs + 50 mg of 9CCN are shown in orange empty squares, SLNs + 100 mg of 9CCN are shown in red triangles and SLNs + 150 mg of 9CCN are shown in purple rectangle. (A) Mean particle size of each formulation (nm). SLNs with 100 mg of 9CCN and 150 mg of 9CCN exhibit disproportionate sizes while SLNs Ctrl, SLNs with 25 mg and 50 mg of 9CCN exhibit an expected and stable size during 48 weeks in both 4 °C and 25 °C. (B) Z-potential was also analyzed in each measurement. SLNs Ctrl, SLNs with 25 mg and 50 mg of 9CCN present an optimal positive potential (between + 25 and + 45 mV) during one year in both temperatures. (C) PDI higher than 0.2 (as in the SLNs 100 mg and 150 mg of 9CCN) indicates different populations of NPs and presence of aggregations.Stability assay was suspended for SLNs + 100 mg and 150 mg of 9CCN due to inappropriate PDI and particle size. **Abbreviations**: Ctrl, control; nm, nanometers; SLNs, solid lipid nanoparticles; 9CCN, cholesteryl-9-carboxynonanoate; NPs, nanoparticles; mV, millivolts; PDI, polydispersion index. (For interpretation of the references to colour in this figure legend, the reader is referred to the web version of this article.)

due to the large change in the ratio of lipid matrix and cationic lipid mix when more than 10 % of 9CCN is added, which alters the morphology of the nanoparticle and favors the appearance of aggregates and dispersed populations, resulting in a suspension of these formulations after 36 weeks. (Fig. 2). Raw data, mean and standard deviation of whole stability assay are presented in Table S2 from Supplementary Information.

As shown in Fig. 3, by TEM we observed the presence of nanostructures with different aggregation and polydisperse properties. While Ctrl and 9CCN-25 mg formulations exhibited spherical and clear presence of NPs, the 9CCN-50 mg showed bigger structures and 9CCN-100 mg or 9CCN-150 mg displayed aggregates and amorphous structures, suggesting the alteration of the cholesteryl oleate or stearic acid moieties and that addition of great amounts of 9CCN to the lipid matrix resulted in unstable SLNs according to PDI analysis.

3.2. Cell viability and binding capacity assays

The cell viability assay of selected SLNs formulations was performed to determine the amount of nanoparticles to be used for the transfection assays. For this purpose, different quantities of SLNs from each formulation (5–25 μL) were added to human HEK293ft cells in 6-well plates, and after 48 h propidium iodide (IP) was added to the 2 mL of DMEM media. Viable cells were quantified by counting the population of non-stained cells by using flow cytometry to discriminate between dead and live cells. We considered toxic effects when cell viability was less than the 80 % observed in mock conditions. Cytotoxicity on HEK293ft cells started to appear at 48 h with volumes higher than 20 μL (for the 9CCN-150 mg formulation) but this was not observed in the case of the other formulations (Fig. 4A). Given that oligonucleotides can alter the physicochemical properties of nanoparticles, we decided to evaluate cell viability also in presence of anti-miR-125b (Figure S1). In this case, only the SLNs 25 mg and 50 mg 9CCN formulations were analyzed as they were the most optimal for further in vitro studies due to their diameter, Z-potential and morphological structures. In the viability assay with the SLNplexes, no toxicity features were observed for these formulations in the same way as with SLNs alone without the anti-miR-125b, thus suggesting that the binding of the antagomir to the nanoparticle does not decrease cell viability. Due to the presence of amorphous structures shown in TEM images and low viability rates, we also decided to discard the 9CCN-150 mg formulation from the next in vitro assays.

Nucleic acid binding capacity to NPs was quantified by adding different amounts of plasmidic DNA (from 500 ng to 3000 ng) to two volumes of SLNs (10 μL or 15 μL). The SLNplexes formed were loaded into an agarose gel in which low binding capacity was evidenced by the presence of free DNA in the gels. We observed high binding efficiency for the SLNs Ctrl, SLNs 9CCN-25 mg and SLNs 9CCN-50 mg with 15 μL of NPs since free DNA could not be detected even after adding 2000 ng of plasmid to SLNs (Fig. 4B). Despite this, the presence of DNA in the condition formed by the SLNs 9CCN-50 mg formulation and 1000 ng of DNA with 10 μL volume suggested to us that this formulation has less binding capacity (Fig. 4C). The fact of modifying the lipid matrix could affect the morphology of the SLN and it may cause the binding capacity to be decreased.

3.3. Cellular transfection and biological activity

Cellular uptake and the ability to produce biological responses were also analyzed for the SLNs Ctrl, SLNs 9CCN-25 mg and SLNs 9CCN-50 mg formulations by combining 12 μL of SLNs with 60 nM of Cy5-labelled antagomiR-125b and transfecting this SLNplex to murine RAW264.7 macrophages. After 48 h flow cytometry analyses showed that the 3 SLNplexes presented high efficiency of transfection compared to control SLNs without Cy5-labelled antagomiR-125b resulting in a high rate of SLNs internalization (Fig. 5A). The cellular internalization of Cy5 antagomiR-125b with the lyophilized SLNs was higher when compared to commercial miRNA transfection lipids (TransIT-X2) but no differences were seen between SLNs Ctrl and SLNs loaded with 9CCN probably due to the phagocytic capacity of macrophages.

We confirmed that SLNs produce a biological effect in the cell other than internalizing nucleic acid, by performing a RT-qPCR. Transfection of SLNplexes (9CCN-25 mg) loaded with the antagomiR-125b resulted in the significant reduction of the expression of the target miRNA-125b, when compared to non-transfected cells (Fig. 5B), thus demonstrating that the fabricated SLNs 9CCN-25 mg had the potential to bind the Cy5-

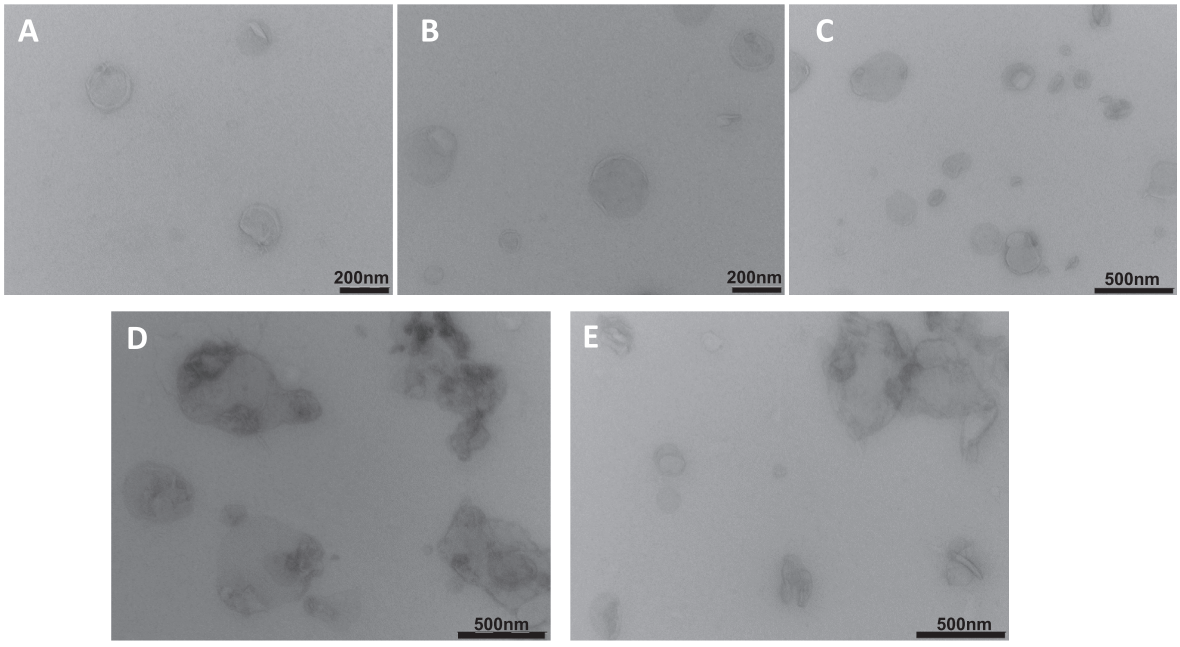

Fig. 3. TEM images of each formulations: (A) SLNs control, (B) SLNs + 25 mg of 9CCN, (C) SLNs + 50 mg of 9CCN, (D) SLNs + 100 mg of 9CCN, (E) SLNs + 150 mg of 9CCN. Formulations A, B and C exhibit a spherical and a clear presence of NPs while in formulations D and E a presence of aggregates and amorphous structures can be observed. Scale bars are shown in black and in nm. **Abbreviations**: TEM, Transmission electron microscopy; nm, nanometers; SLNs, solid lipid nanoparticles; 9CCN, cholesteryl-9-carboxynonanoate; NPs, nanoparticles.

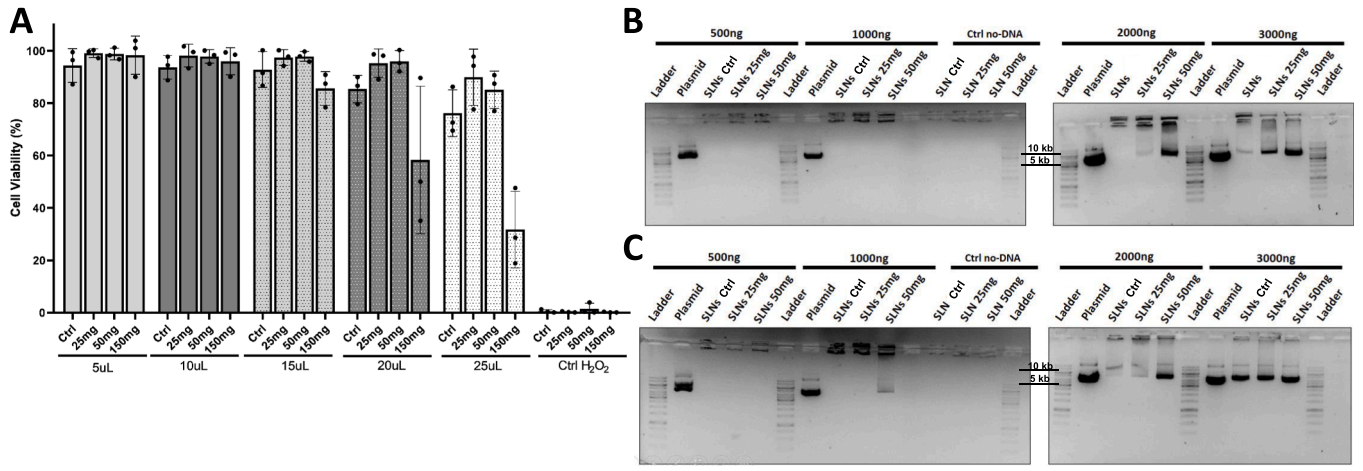

Fig. 4. (A) Cell viability assay in HEK293ft cells with different volumes of SLNs Ctrl, SLNs + 25 mg of 9CCN, SLNs + 50 mg of 9CCN and SLNs + 150 mg of 9CCN formulations. Volumes from 20 μL of SLNs + 150 mg of 9CCN have a low cell viability profile. Data are from three independent experiments (mean + SD). (B) Agarose gel electrophoresis of 15 μL or (C) 10 μL of SLNs:pDNA lipoplexes. 500 ng to 3000 ng of pDNA was mixed with SLNs Ctrl, SLNs + 25 m 9CCN and SLNs + 50 mg 9CCN and were loaded into 0.8 %. The presence of free DNA revealed the binding capacity of the NPs which was supported with control loaded SLNs without DNA or control plasmid with DNA. Ladder showed molecular-weight size marker in kb pairs. **Abbreviations**: Ctrl, control; SLNs, solid lipid nanoparticles; 9CCN, cholesteryl-9-carboxynonanoate; pDNA, plasmid DNA; NPs, nanoparticles; kb, kilobase; HEK293, human embryonic kidney 293 cells; SD, standard deviation; H_2O_2, hydrogen peroxide.

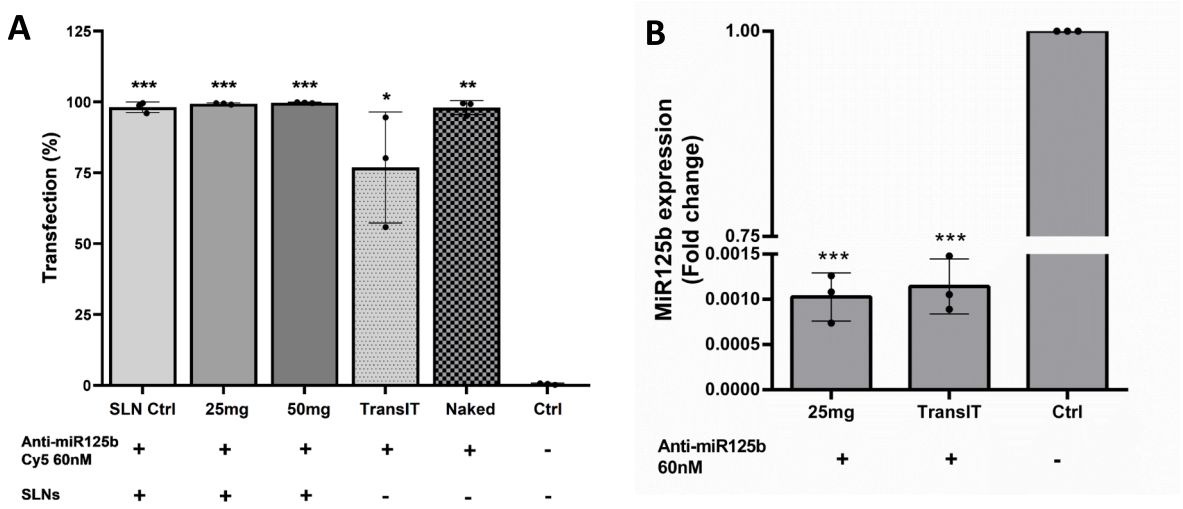

Fig. 5. (A) Transfection efficiency of 60 nM Cy5-AntagomiR125b with SLNs Ctrl, with SLNs + 25 mg 9CCN, with SLNs + 50 mg 9CCN, with commercial TransIT-X2 (Mirusbio, USA) or naked into RAW264.7 cells at 48 h. Statistically significative differences in SLNs transfection were observed compared to non-transfected control. Flow cytometry histograms showing transfection efficiency are presented in Figure S4. (B) Biological activity of the anti-miRNA125b transfected into RAW264.7 cells at 60 nM was assessed analyzing the expression of the miR125b by RT-qPCR. SLNs + 25 mg of 9CCN presented a notable inhibition of the miR125b compared to non-transfected control. Experiments were performed in triplicate (mean + SD). *** $P < 0.001$, ** $P = 0.01–0.001$, * $P < 0.01$. **Abbreviations**: Ctrl, control; SLNs, solid lipid nanoparticles; 9CCN, cholesteryl-9-carboxynonanoate; Cy5, cyanine 5; SD, standard deviation; ctrl, control.

antagomiR-125b, to internalize it, release it and targeting miR-125b.

Cellular uptake was also supported by the observation of transfected cells with the confocal microscopy as shown in Fig. 6. At 2 h post-transfection, a fluorescence signal was detected in all formulations and the commercial transfection reagent control, suggesting that internalization of SLNplexes occurs promptly. Fluorescence signal was highly increased after 24 h post-transfection reflecting that delivered nucleic acid was internalized. Moreover, transfection with SLNs 9CCN-25 mg and Cy5_antagomiR-125b resulted in the strongest signal of fluorescence (Fig. 6B) even when compared to commercial lipo-transfection agent, revealing that this might be the best formulation to direct the antagomiR-125b to the target cell.

3.4. SLNs as in vivo delivery system and targeting to macrophages

To demonstrate the selective delivery to macrophages we administered SLNplexes to ApoE-/- mice. Based on previous data on stability, viability and biological response, the 9CCN-25 mg SLNs formulation was chosen as candidate for the in vivo experiments. The 9CCN-50 mg SLNs formulation could be also a good candidate for in vivo studies, but due to the alterations in morphology, diameter and dispersion observed in formulations with higher ratio of 9CCN to the original lipid matrix, we decided to choose the formulation with 25 mg of 9CCN for these preliminary in vivo trials. The 25 mg formulation is the best candidate as the composition of the original lipid matrix is not exaggeratedly altered, demonstrates selectivity and high transfection capacity in vitro and may

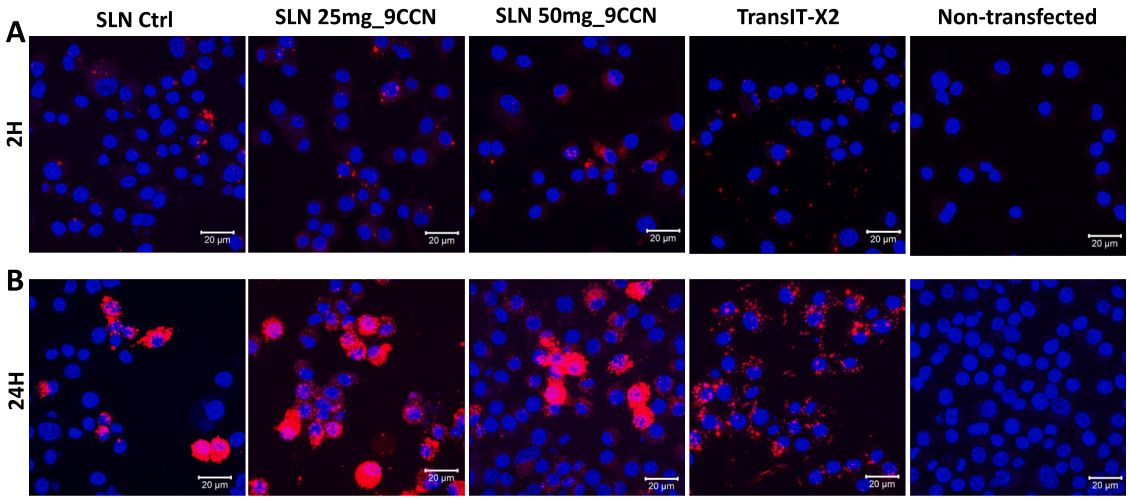

Fig. 6. Confocal microscopy images of RAW264.7 cells transfected with 60 nM Cy5-AntagomiR125b forming lipoplexes with SLN Ctrl, SLNs + 25 mg of 9CCN, SLNs + 50 mg of 9CCN, commercial TransIT-X2 or non-transfected after 2 h (A, upper images) or 24 h (B, lower images) post-transfection. Blue, DAPI staining; red, Cy5-labeled antagomiR125b. Scale bars are shown in white and in 20 µm. **Abbreviations**: Ctrl, control; SLNs, solid lipid nanoparticles; 9CCN, cholesteryl-9-carboxynonanoate; Cy5, cyanine 5; DAPI, 4′,6-damidino-2-phenylindole. (For interpretation of the references to colour in this figure legend, the reader is referred to the web version of this article.)

also be a good choice in terms of industrial scalability as less 9CCN is used.

SLNplexes carrying 15 mg/kg of Cy5-labeled antagomiR-125b were administered to ApoE-/- mice subcutaneously once per week while one dose of 15 mg/kg "naked", Cy5-labeled, antagomiR-125b was administered as control. After 24 h, fluorescence microscopy revealed that naked antagomiR-125b remained under the injection site, whereas in the SLNs group, antagomiR-125b labeling was less intense, suggesting faster distribution (Fig. 7A). In addition, antagomiR-125b-loaded SLNs demonstrated a remarkable ability to selectively target macrophages within atheroma lesions (Fig. 7D). Furthermore, these SLNs have also exhibited effective uptake by renal tubular cells (Fig. 7B).

In addition, quantitative analyses were performed to allow us to contrast the qualitative findings of the confocal microscopy. ImageJ analysis revealed that the group treated with SLNs and anti-miR-125b showed significant differences ($p = 0.05$) with respect to the anti-miR-125b naked group in terms of the number of positive cells at the aortic valve level in the atheroma plaque (Fig. 8B). This demonstrates that SLNs are more selective for macrophages overexpressing miR-125b, as there is more presence of labeled anti-miR-125b within the aortic valve atheroma plaque. In addition, real-time quantitative PCR was performed in cDNA from 3 different tissues: aorta, kidney and PBMCs comparing the naked group vs SLNs-treated group. The results showed that in both kidney ($p = 0.20$) and aorta ($p = 0.20$), there is less expression of miR-125b, so with SLNs more anti-miR-125b could arrive to the tissue. The PBMCs from the bone marrow of both groups were also

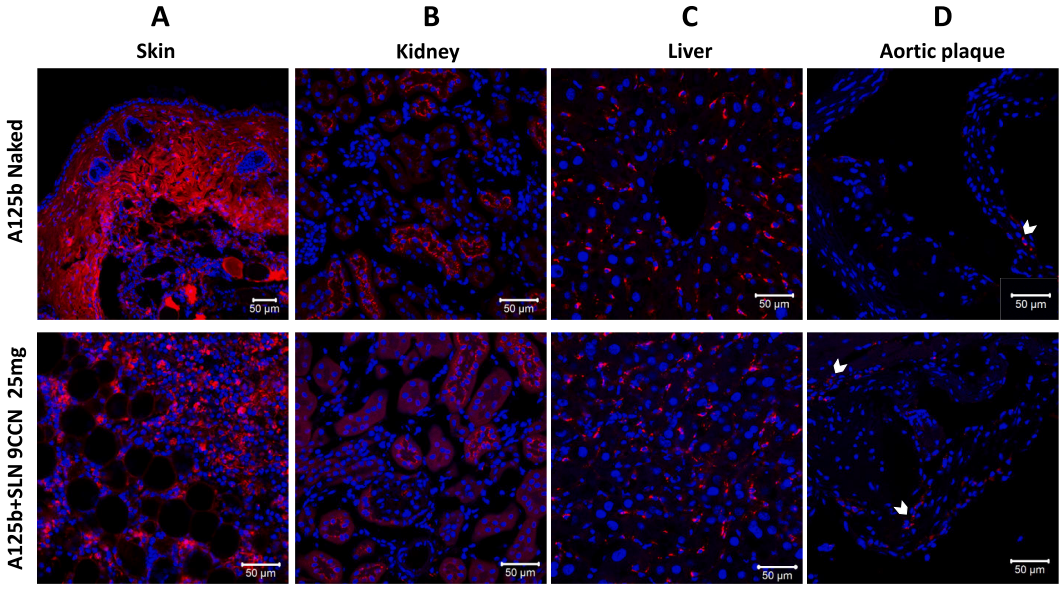

Fig. 7. Confocal microscopy images of OCT-embedded tissues from ApoE-/- mice subcutaneously treated with 1 dose of Cy5-loaded antagomiR-125b alone (upper images) or together with SLNs + 25 mg of 9CCN resuspended and filtered formulations. Presence of A125b is shown in red in the site of injection (A), in tubular cells from kidney (B), in hepatocytes and Kupffer cells from the liver (C) and in the macrophages of an atheroma plaque from aortic valve (D, white arrows). Blue, DAPI staining; red, Cy5-labeled antagomiR125b. Scale bars are shown in white and in 50 µm. **Abbreviations**: Ctrl, control; SLNs, solid lipid nanoparticles; 9CCN, cholesteryl-9-carboxynonanoate; Cy5, cyanine 5; DAPI, 4′,6-damidino-2-phenylindole; A125b, antagomiR-125b. (For interpretation of the references to colour in this figure legend, the reader is referred to the web version of this article.)

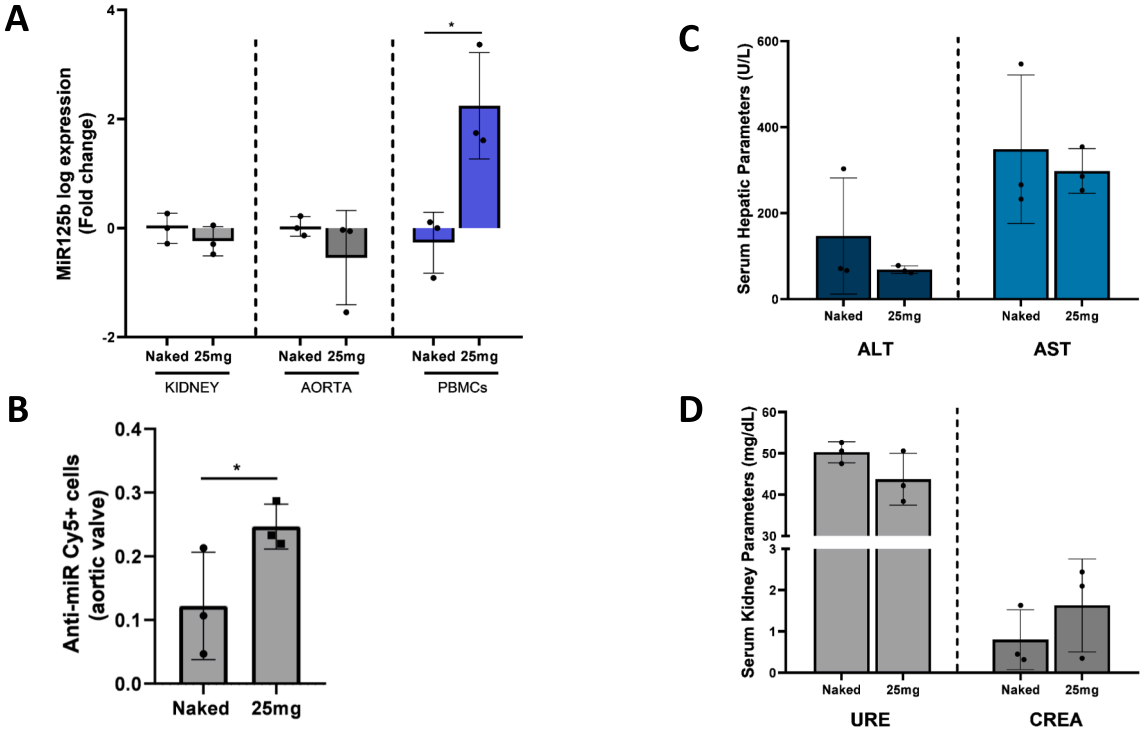

Fig. 8. Quantitative analysis of in vivo experiments. (A) Mir-125b log expression in Kidney, Aorta and PBMCs tissues from naked anti-miR125b mice group or SLNs + anti-miR125b mice group assessed by RT-qPCR. SLNs + 25 mg of 9CCN group presented a notable inhibition of the miR125b compared to naked group in Aorta and Kidney. SLNs + 25 mg 9CCN group also present less miR-125b inhibition in PBMCs from bone marrow, suggesting less off-target effects. Unpaired *t*-test two-tailed was performed for kidney and PBMCs and Mann Whitney non-parametric test was performed for aorta. * $P \leq 0.05$. (B) ImageJ quantification of positive anti-miR125b Cy5 marked cells. Mann Whitney non-parametric test one-tailed was performed. * $P \leq 0.05$. (C) Serum levels ALT and AST from ApoE-/- mice treated with A125b naked or with SLNs + 25 mg of 9CCN. No differences regarding hepatotoxicity were observed. (D) Serum levels Creatinine and Urea from ApoE-/- mice treated with A125b naked or with SLNs + 25 mg of 9CCN. No differences regarding nephrotoxicity were observed. Two-way ANOVA followed by Sidak's correction was performed for serum quantification ($P > 0.05$). **Abbreviations**: SLNs, solid lipid nanoparticles; 9CCN, cholesteryl-9-carboxynonanoate; PBMCs, Peripheral blood mononuclear cells; RT-qPCR, real time quantitative polymerase chain reaction; ALT, Alanine transaminase; AST, Aspartate transaminase; CREA, Creatinine; URE, Urea.

analyzed, observing that in the SLNs-treated group there is greater expression of miR-125b ($p = 0.018$) with respect to the naked group, suggesting that SLNs are more selective and for this reason do not reach the bone marrow, avoiding an off-target effect. (Fig. 8A).

Toxicity of in vivo SLNs administration was also evaluated by quantifying serum markers ALT, AST, Creatinine and Urea (Fig. 8C, 8D) from SLNs and naked groups. The results showed no significative differences between SLNplex groups versus naked group, indicating that SLNs do not produce hepatic nor kidney toxicity. The group treated with SLNs even had slightly lower ALT ($p = 0.661$), AST ($p = 0.836$) and Urea ($p = 0.096$) levels when compared with the group treated without SLNs. Although creatinine is the only parameter slightly higher in the group treated with SLNs, the differences are not significant either ($p = 0.949$). These findings indicate the potential of SLNs-9CCN as promising nanocarriers for the delivery of target treatments for both ATH and renal diseases.

4. Discussion

Specific nucleic acid delivery has been one of the main challenges for the use of nanotechnology in therapy [6]. Over two decades, SLNs have been proved as one of the most advantageous drug nanocarriers compared to other polymeric NPs, emulsions or liposomes, playing a central role in the delivery of short nucleic acids (i.e. siRNA) and mRNA-based vaccines into target cells. An example of this is Patisiran, a lipid nanoparticle-formulated siRNA, which was approved in 2018 under the trade name of Onpattro to treat hereditary transthyretin amyloidosis (hARRT) [36]. Recent clinical trials also reported the intramuscular administration of lipid nanoparticle-formulated mRNA as vaccine prevention of COVID-19 by using an mRNA that encodes the SARS-CoV-2 spike protein (i.e. Tozinameran under the trade name Comirnaty or Elasomeran under the trade name of Spikevax, both approved in 2020) as described by Suzuki and Ishihara [37]). The solid lipid structures of these NPs provided chemical stability of the cargo, further offering its controlled release and conferring a reduced cytotoxicity because of the safe and physiologically well-tolerated components in dermal, oral and intravenous applications [38]. However, in vivo trafficking and delivery to extrahepatic target cells remain a concern to be improved due to NP main clearance by the liver and the following lack of nucleic acid arrival to the desired tissue [16]. Thus, there is an urgent need to improve the SLNs in vivo fate and release rate of the cargo.

The aim of this study was to optimize the fabrication of an improved type of SLNs incorporating the 9CCN lipid "eat-me" signalfor targeting macrophages and achieve higher rates of antagomiR delivery. We hypothesized that adding cholesterol-derived lipids in the lipid matrix should not change the morphology nor the membrane potential and we decided the 9CCN as a candidate since PtdSer molecule is negatively charged and may affect the antagomiR binding to the nanoparticle [31,39]. Avoiding aggregates, staying within the diameter and positive charge surface of meticulously developed SLNs were the main factors for considering when we decided the 4 formulations [23]): 25 mg of 9CCN, 50 mg of 9CCN, 100 mg of 9CCN and 150 mg of 9CCN. According to previous studies (Fàbregas A et al. 2017; Suñé M et al. 2019), we sought to obtain nanoparticles around 200 nm diameter because they exhibited

less cytotoxicity and higher rates of cell transfection. Moreover, nanoparticles with Z-potential values between 25 and 40 mV are required for good capacity of nucleic acid binding in a highly stable colloidal system.".

The first objective of this study was to assess the morphology and stability of four fabricated formulations, and we have shown that SLNs containing 25 mg of 9CCN and 50 mg of 9CCN present spherical structures according to electron microscopy and can be conveniently resuspended within the 1st year of lyophilization preserving the positive + 25–40 mV Z-potential in surface and diameter around 200 nm without presenting aggregates. While 25 mg and 50 mg 9CCN formulations showed spherical structures in electron microscopy and low levels of cytotoxicity, formulations with high concentration of 9CCN presented amorphous structures of NPs, aggregations and less cell viability suggesting that variations in lipid matrix might destabilize the structure of nanoparticles [23,40]. Transfection efficiency and biological response into cellular lines was also a point to analyze in this study and these formulations showed a good binding capacity for nucleic acid union and cytometry and confocal microscopy proved the ability they presented for the delivery of antagomiR into the macrophages RAW264.7 cell line. Interestingly, cationic 9CCN-based SLNs might protect the antagomiR SLNplex to degradation and allow a rapid uptake within the first 2 h with more than 90 % of oligonucleotide incorporation to the cell, which outperforms other SLNs formulations positioning itself as a novel in vitro transfection reagent and non-viral system [41,42].

In vivo antagomiR degradation by nucleases has been a potential challenge for oligonucleotide modifications and nanocarrier development [43,44]. Much effort has been dedicated in the development of nanoparticles for loading miRNA antagonists and have shown promising results in different disease mice models [45–47], including atherosclerosis as shown in Chin et al [48] study. Alternatively, novel methods for RNA-delivery such as creation of pH-regulated NPs, peptide-loaded nanocarriers for oral delivery or biomimetic viral-based and bacterial-based NPs have been emerged [49–51]. Despite all these advantages, one of the major problems in the use of nanoparticles is the off-target effects. The biodistribution of nanoparticles remains a current challenge as many lipid nanoparticles accumulate in hepatocytes and Kupffer cells or are unable to cross some endothelial barriers. The findings from our in vivo results indicated that for the first time, SLNs 9CCN-based nanoformulations allow the delivery of therapeutic oligonucleotide anti-miRNA125b loaded with Cyanine-5 in ApoE-/- mice model, thus proving its effect in targeting miR-125b, being uptaken by the macrophages from atheroma plaque at the level of aortic valves. The effectiveness of nanoparticle targeting was also demonstrated by RT-qPCR results. The group of mice treated with anti-miR125b + SLN showed more inhibition of miR-125b expressed mainly in macrophages in both aorta and kidney and less inhibition in PBMCs meaning that it does not reach the bone marrow and avoiding the off-target effect that occurs in the naked mice group. These results provide further evidence that by modulating the lipid structure of the nanoparticle surface cholesterol to 9CCN, the lipid nanoparticle is able to achieve cell-specific delivery of oligonucleotide in macrophages. Besides the good results in macrophage selectivity, long-term biodistribution studies at the in vivo level should be performed.

Our in vivo study also shown the antagomiR-125b metabolism via hepatocytes cells including Kupffer cells and the antagomiR-125b reabsorption in tubular kidney cells, suggesting that 9CCN SLNs may be an efficient delivery system for transporting drugs or nucleic acids in an extrahepatic way to the kidney. The rapid absorption of antagomiR125b when administered subcutaneously by SLNs compared to naked administration highlights the role of inflammatory process in distribution and selectively delivery of antagomiR loaded SLNs corroborating the results obtained by the in vitro assays. Furthermore, the evaluation of serum toxicity parameters ALT, AST, Creatinine and Urea showed no significant differences between the SLNs or naked treated group therefore the addition of nanoparticles does not imply an added harm to the mice. Although the good results of toxicity and distribution of SLNs in 24 h cannot be generalized to long-term therapeutic results. Continued long-term administration of SLNs (e.g. 6 months) may cause undesirable accumulation leading to cytotoxicity. Therefore, RNA-seq analysis of cell types from different tissues where SLNs bioaccumulate will be a challenge for our next studies to understand the relationship between the properties of the nanoparticle with its biodistribution. Meticulous observation is required to see whether the antagomiR taken up by the in vivo cells produces the same biological action that is observed in the in vitro cell lines within a long period of time. In addition, the choice of other biodegradable lipids may be a good parameter to consider for the fabrication of lipid nanoparticles in the future. Biodegradable lipids are part of the COVID-19 mRNA vaccine and help to remove the nanoparticles faster from plasma and tissue helping to improve tolerability and safety.

Moreover, further studies will be required in order to determine whether SLNs fabrication brings more benefits in terms of manufacturing costs and in a scale-up process. Large scale fabrication and manufacturing of lipid nanoparticles according to CGMP remain both challenging and complex as NP equipment and molecules used for excipients sometimes are not considered fit for purpose. Standardization and scalability are critical path activities for SLN manufacturing. The reproducibility of diameter and nucleic acid binding capacity of SLNs alongside with bioavailability and stability studies are also an urgent need before moving to clinical trials. The lyophilization process used in this work and the stability assay in both 4 °C and 25 °C, could act as precedent for future attempts to industrialize SLNs that incorporate new modified lipids. Taken together, the new formulations of SLNs incorporating lower quantities of 9CCN loaded with antisense oligonucleotides can efficiently target macrophages and might result in an improvement of in vivo off-target effects that will enhance the selectively delivery within mice models.

5. Conclusions

Lipid nanoparticles have been considered a good nucleic acid delivery system, many attempts have been made to improve their immunogenicity, cytotoxicity and nucleic acid delivery. The incorporation of a lipid "eat-me" signal to SLNs has allowed directing these nanocarriers loaded with an antagomiR to target cells. The SLNs + 25 mg of 9CCN formulation was considered the best NP that reached the optimal size, Z-potential and PDI during 48 weeks since its lyophilization. Moreover, the cell viability and binding capacity presented a good profile which was reflected within the in vitro transfection assays and ApoE-/- mice SLNplexes administration showed promising results in releasing the anti-miRNA thus encouraging further research using in vivo models.

CRediT authorship contribution statement

Adrian Mallén: Writing – review & editing, Writing – original draft, Visualization, Project administration, Methodology, Investigation, Formal analysis, Data curation, Conceptualization. **David A. Narváez-Narváez:** Methodology, Investigation, Formal analysis. **M.D. Pujol:** Investigation. **Estanis Navarro:** Writing – review & editing, Writing – original draft, Visualization, Formal analysis, Data curation, Conceptualization. **Josep Maria Suñé-Negre:** Resources, Project administration, Methodology, Funding acquisition, Data curation, Conceptualization. **Encarna García-Montoya:** Investigation. **Pilar Pérez-Lozano:** Investigation. **Benjamín Torrejón-Escribano:** Formal analysis. **Marc Suñé-Pou:** Writing – review & editing, Writing – original draft, Visualization, Validation, Supervision, Methodology, Investigation, Formal analysis, Data curation, Conceptualization. **Miguel Hueso:** Writing – review & editing, Writing – original draft, Visualization, Supervision, Resources, Project administration, Methodology, Investigation, Funding acquisition, Formal analysis, Data curation, Conceptualization.

Declaration of competing interest

The authors declare that they have no known competing financial interests or personal relationships that could have appeared to influence the work reported in this paper.

Data availability

Data will be made available on request.

Acknowledgements

This study has been partially funded by Instituto de Salud Carlos III (Co-funded by European Regional Development Fund. ERDF, a way to build Europe) through the project PI 18/01108 and the project PI23/00927 to MH and by RICORS (RD21/0005/0001). We thank the CERCA program/ Generalitat de Catalunya for institutional support and the Service of Pharmacology, Toxicology and Therapeutic Chemistry from University of Barcelona for their knowledge and machinery in nanoparticle fabrication. We also thank the Bellvitge Unit from Scientific and Technological Centers (CCiTUB), Universitat de Barcelona, and Maria Esther Castaño for their support and advice on flow cytometry technique.

Appendix A. Supplementary data

Supplementary data to this article can be found online at https://doi.org/10.1016/j.ejpb.2024.114238.

References

[1] M. Kowara, S. Borodzicz-Jazdzyk, K. Rybak, M. Kubik, A. Cudnoch-Jedrzejewska, Therapies targeted at non-coding RNAs in prevention and limitation of myocardial infarction and subsequent cardiac remodeling-current experience and perspectives [cited 2023 Jul 5], Available from: Int. J. Mol. Sci.. [internet]. 22 (11) (2021).
[2] T. Lobovkina, G.B. Jacobson, E. Gonzalez-Gonzalez, R.P. Hickerson, D. Leake, R. L. Kaspar, et al., In vivo sustained release of siRNA from solid lipid nanoparticles [cited 2023 Jul 5], Available from: ACS Nano [Internet]. 5 (12) (2011) 9977–9983.
[3] R.C. Lee, R.L. Feinbaum, V. Ambros, The C. elegans heterochronic gene lin-4 encodes small RNAs with antisense complementarity to lin-14 [cited 2023 Jul 5], Available from: Cell [Internet]. 75 (5) (1993) 843–854.
[4] E. Navarro, A. Mallén, M. Hueso, Dynamic Variations of 3'UTR Length Reprogram the mRNA Regulatory Landscape [cited 2023 Jul 5], Available from: Biomedicines [Internet]. 9 (11) (2021).
[5] S. De Benedittis, F. Fortunato, C. Cava, F. Gallivanone, E. Iaccino, M.E. Caligiuri, et al., Circulating microRNA: The Potential Novel Diagnostic Biomarkers to Predict Drug Resistance in Temporal Lobe Epilepsy, a Pilot Study [cited 2023 Jul 4], Available from: Int J Mol Sci [Internet]. 22 (2) (2021) 1–15.
[6] M. Hueso, A. Mallén, M. Suñé-pou, J.M. Aran, J.M. Suñé-negre, E. Navarro, ncRNAs in Therapeutics: Challenges and Limitations in Nucleic Acid-Based Drug Delivery [cited 2023 Jul 5], Available from: Int J Mol Sci [Internet]. 22 (21) (2021).
[7] R. Kole, A.R. Krainer, S. Altman, RNA therapeutics: beyond RNA interference and antisense oligonucleotides [cited 2023 Jul 5], Available from: Nat Rev Drug Discov [Internet]. 11 (2) (2012) 125–140.
[8] R. Rupaimoole, discovery FSN reviews D, 2017 undefined. MicroRNA therapeutics: towards a new era for the management of cancer and other diseases. nature.com [Internet]. 2017 [cited 2023 Jul 5]; Available from: https://www.nature.com/articles/nrd.2016.246.
[9] K.A. Lennox, M.A. Behlke, Chemical modification and design of anti-miRNA oligonucleotides [cited 2023 Jul 5], Available from: GeneTher [Internet]. 18 (12) (2011) 1111–1120.
[10] R.L. Juliano, The delivery of therapeutic oligonucleotides [cited 2023 Jul 5], Available from: Nucleic Acids Res [Internet]. 44 (14) (2016) 6518–6548.
[11] K.S. Park, X. Sun, M.E. Aikins, J.J. Moon, Non-viral COVID-19 vaccine delivery systems [cited 2023 Jul 5], Available from: Adv Drug Deliv Rev [Internet]. 169 (2021) 137–151.
[12] T.C. Roberts, R. Langer, M.J.A. Wood, Advances in oligonucleotide drug delivery [cited 2023 Jul 5], Available from: Nat Rev Drug Discov [Internet]. 19 (10) (2020) 673–694.
[13] S.W.L. Lee, C. Paoletti, M. Campisi, T. Osaki, G. Adriani, R.D. Kamm, et al., MicroRNA delivery through nanoparticles [cited 2023 Jul 5], Available from: J Control Release [Internet]. 313 (2019) 80–95.
[14] P. Velpurisiva, A. Gad, B. Piel, R. Jadia, P. Rai, Nanoparticle Design Strategies for Effective Cancer Immunotherapy [cited 2023 Jul 5], Available from: J Biomed (Syd) [Internet]. 2 (2) (2017) 64–77.
[15] P. Decuzzi, B. Godin, T. Tanaka, S.Y. Lee, C. Chiappini, X. Liu, et al., Size and shape effects in the biodistribution of intravascularly injected particles [cited 2023 Jul 5], Available from: J Control Release [internet]. 141 (3) (2010) 320–327 https://pubmed.ncbi.nlm.nih.gov/19874859/.
[16] T. Nakamura, Y. Sato, Y. Yamada, M.M. Abd Elwakil, S. Kimura, M.A. Younis, et al., Extrahepatic targeting of lipid nanoparticles in vivo with intracellular targeting for future nanomedicines [cited 2023 Jul 5], Available from: Adv Drug Deliv Rev [Internet]. 188 (2022).
[17] T. Zhang, X. Xue, D. He, J.T. Hsieh, A prostate cancer-targeted polyarginine-disulfide linked PEI nanocarrier for delivery of microRNA [cited 2023 Jul 5], Available from: Cancer Lett [Internet]. 365 (2) (2015) 156–165.
[18] A. Ekin, O.F. Karatas, M. Culha, M. Ozen, Designing a gold nanoparticle-based nanocarrier for microRNA transfection into the prostate and breast cancer cells [cited 2023 Jul 5], Available from: J Gene Med [Internet]. 16 (11–12) (2014) 331–335.
[19] C. He, Y. Hu, L. Yin, C. Tang, C. Yin, Effects of particle size and surface charge on cellular uptake and biodistribution of polymeric nanoparticles [cited 2023 Jul 5], Available from: Biomaterials [internet]. 31 (13) (2010) 3657–3666.
[20] A. Mohamed, N.K. Kunda, K. Ross, G.A. Hutcheon, I.Y. Saleem, Polymeric nanoparticles for the delivery of miRNA to treat Chronic Obstructive Pulmonary Disease (COPD) [cited 2023 Jul 5], Available from: Eur J Pharm Biopharm [internet] 136 (2019) 1–8 https://pubmed.ncbi.nlm.nih.gov/30615927/.
[21] J.P. Rao, K.E. Geckeler, Polymer nanoparticles: Preparation techniques and size-control parameters, Prog Polym Sci. 36 (7) (2011) 887–913.
[22] H. Lv, S. Zhang, B. Wang, S. Cui, J. Yan, Toxicity of cationic lipids and cationic polymers in gene delivery [cited 2023 Jul 5], Available from: J Control Release [Internet]. 114 (1) (2006) 100–109.
[23] M. Suñé-Pou, S. Prieto-Sánchez, Y. El Yousfi, S. Boyero-Corral, A. Nardi-Ricart, I. Nofrerias-Roig, et al., Cholesteryl oleate-loaded cationic solid lipid nanoparticles as carriers for efficient gene-silencing therapy [cited 2023 Jul 5], Available from: Int J Nanomedicine [Internet] 13 (2018) 3223–3233.
[24] A. Fàbregas, S. Prieto, M. Suñé-Pou, S. Boyero-Corral, J.R. Ticó, E. García-Montoya, et al., Improved formulation of cationic solid lipid nanoparticles displays cellular uptake and biological activity of nucleic acids [cited 2023 Jul 5], Available from: Int J Pharm [Internet]. 516 (1–2) (2017) 39–44.
[25] M.J. Limeres, M. Suñé-Pou, S. Prieto-Sánchez, C. Moreno-Castro, A.D. Nusblat, C. Hernández-Munain, et al., Development and characterization of an improved formulation of cholesteryl oleate-loaded cationic solid-lipid nanoparticles as an efficient non-viral gene delivery system [cited 2023 Jul 5], Available from: Colloids Surf. B BiointerfacesBiointerfaces [Internet]. (2019) 184.
[26] J. Zhang, Y. Zu, C.S. Dhanasekara, J. Li, D. Wu, Z. Fan, et al., Detection and treatment of atherosclerosis using nanoparticles [cited 2023 Jul 5], Available from: Wiley Interdiscip Rev Nanomed Nanobiotechnol [Internet]. 9 (1) (2017).
[27] M. Hueso, L. De Ramon, E. Navarro, E. Ripoll, J.M. Cruzado, J.M. Grinyo, et al., Silencing of CD40 in vivo reduces progression of experimental atherogenesis through an NF-κB/miR-125b axis and reveals new potential mediators in the pathogenesis of atherosclerosis [cited 2023 Jul 5], Available from: Atherosclerosis [Internet]. 255 (2016) 80–89.
[28] M. Hueso, R. Griñán, A. Mallen, E. Navarro, E. Purqueras, M. Gomá, et al., MiR-125b downregulates macrophage scavenger receptor type B1 and reverse cholesterol transport [cited 2023 Jul 5], Available from: Biomed Pharmacother [Internet]. 146 (2022).
[29] Chao C. Ter, H.Y. Yeh, T.H. Yuan, C.K. Chiang, H.W. Chen, MicroRNA-125b in vascular diseases: An updated systematic review of pathogenetic implications and clinical applications [cited 2023 Jul 4], Available from: J Cell Mol Med [Internet]. 23 (9) (2019) 5884–5894.
[30] V. Bagalkot, J.A. Deiuliis, S. Rajagopalan, A. Maiseyeu, "Eat me" imaging and therapy, Adv. Drug. Deliv. Rev. [Internet], 99(Pt A) (2016) 2–11. [cited 2023 Jul 4], Available from: https://pubmed.ncbi.nlm.nih.gov/26826436/.
[31] W. Li, Eat-me signals: keys to molecular phagocyte biology and "appetite" control [cited 2023 Jul 5], Available from: J Cell Physiol [Internet]. 227 (4) (2012) 1291–1297.
[32] A. Maiseyeu, G. Mihai, S. Roy, N. Kherada, O.P. Simonetti, C.K. Sen, et al., Detection of macrophages via paramagnetic vesicles incorporating oxidatively tailored cholesterol ester: an approach for atherosclerosis imaging [cited 2023 Jul 5], Available from: Nanomedicine (Lond) [Internet]. 5 (9) (2010) 1341–1356.
[33] V. Bagalkot, M.A. Badgeley, T. Kampfrath, J.A. Deiuliis, S. Rajagopalan, A. Maiseyeu, Hybrid nanoparticles improve targeting to inflammatory macrophages through phagocytic signals [cited 2023 Jul 4], Available from: J Control Release [Internet]. 217 (2015) 243–255.
[34] A. Fàbregas, N. Sánchez-Hernández, J.R. Ticó, E. García-Montoya, P. Pérez-Lozano, J.M. Suñé-Negre, et al., A new optimized formulation of cationic solid lipid nanoparticles intended for gene delivery: development, characterization and DNA binding efficiency of TCERG1 expression plasmid [cited 2023 Jul 5], Available from: Int. J. Pharm. [Internet]. 473 (1–2) (2014) 270–279.
[35] E. Vighi, B. Ruozi, M. Montanari, R. Battini, E. Leo, pDNA condensation capacity and in vitro gene delivery properties of cationic solid lipid nanoparticles [cited 2023 Jul 5], Available from: Int J Pharm [Internet]. 389 (1–2) (2010) 254–261.
[36] D. Adams, A. Gonzalez-Duarte, W.D. O'Riordan, C.C. Yang, M. Ueda, A.V. Kristen, et al., Patisiran, an RNAi Therapeutic, for Hereditary Transthyretin Amyloidosis [cited 2023 Jul 4], Available from: N Engl J Med [Internet]. 379 (1) (2018) 11–21.
[37] Y. Suzuki, H. Ishihara, Difference in the lipid nanoparticle technology employed in three approved siRNA (Patisiran) and mRNA (COVID-19 vaccine) drugs [cited 2023 Jul 5], Available from: Drug Metab Pharmacokinet [Internet]. (2021) 41.

[38] L. Bayón-Cordero, I. Alkorta, L. Arana, Application of Solid Lipid Nanoparticles to Improve the Efficiency of Anticancer Drugs [cited 2023 Jul 4], Available from: Nanomaterials (Basel) [Internet]. 9 (3) (2019).
[39] A. Matsumoto, Y. Takahashi, M. Nishikawa, K. Sano, M. Morishita, C. Charoenviriyakul, et al., Role of Phosphatidylserine-Derived Negative Surface Charges in the Recognition and Uptake of Intravenously Injected B16BL6-Derived Exosomes by Macrophages [cited 2023 Jul 5], Available from: J. Pharm.Sci [Internet]. 106 (1) (2017) 168–175.
[40] D. Pozzi, C. Marchini, F. Cardarelli, H. Amenitsch, C. Garulli, A. Bifone, et al., Transfection efficiency boost of cholesterol-containing lipoplexes [cited 2023 Jul 5], Available from: Biochim Biophys Acta [Internet]. 1818 (9) (2012) 2335–2343.
[41] E. Vighi, M. Montanari, M. Hanuskova, V. Iannuccelli, G. Coppi, E. Leo, Design flexibility influencing the in vitro behavior of cationic SLN as a nonviral gene vector [cited 2023 Jul 5], Available from: Int J Pharm [Internet]. 440 (2) (2013) 161–169.
[42] R. Cortesi, M. Campioni, L. Ravani, M. Drechsler, M. Pinotti, E. Esposito, Cationic lipid nanosystems as carriers for nucleic acids [cited 2023 Jul 4], Available from: N Biotechnol [Internet]. 31 (1) (2014) 44–54.
[43] B. Duygu, R. Juni, L. Ottaviani, N. Bitsch, J.B.M. Wit, L.J. de Windt, et al., Comparison of different chemically modified inhibitors of miR-199b in vivo [cited 2023 Jul 5], Available from: Biochem. Pharmacol [Internet]. 159 (2019) 106–115.
[44] H. Guo, K. Yoshioka, T. Kunieda, Y. Asami, H. Miyata, K. Yoshida-Tanaka, et al., Efficacy of microRNA silencing by lipid-conjugated double-stranded antisense oligonucleotides, J. Med. Dent. Sci. 65 (2) (2018) 83–88.
[45] R. Chaudhari, S. Nasra, N. Meghani, A. Kumar, MiR-206 conjugated gold nanoparticle based targeted therapy in breast cancer cells [cited 2023 Jul 4], Available from: Sci Rep [Internet]. 12 (1) (2022).
[46] M.S. Song, J.J. Rossi, The anti-miR21 antagomir, a therapeutic tool for colorectal cancer, has a potential synergistic effect by perturbing an angiogenesis-associated miR30 [cited 2023 Jul 5], Available from: Front Genet [Internet]. 4 (JAN) (2014).
[47] Y. Wang, Y. Xie, K.V. Kilchrist, J. Li, C.L. Duvall, D. Oupický, Endosomolytic and Tumor-Penetrating Mesoporous Silica Nanoparticles for siRNA/miRNA Combination Cancer Therapy [cited 2023 Jul 5], Available from: ACS Appl Mater Interfaces [Internet]. 12 (4) (2020) 4308–4322.
[48] D.D. Chin, C. Poon, J. Wang, J. Joo, V. Ong, Z. Jiang, et al., miR-145 micelles mitigate atherosclerosis by modulating vascular smooth muscle cell phenotype [cited 2023 Jul 4], Available from: Biomaterials [Internet]. (2021) 273.
[49] B. Chen, L. Mei, Y. Wang, G. Guo, Advances in intelligent DNA nanomachines for targeted cancer therapy [cited 2023 Jul 4], Available from: Drug Discov Today [Internet]. 26 (4) (2021) 1018–1029.
[50] S.K. Dubey, S. Parab, N. Dabholkar, M. Agrawal, G. Singhvi, A. Alexander, et al., Oral peptide delivery: challenges and the way ahead [cited 2023 Jul 5], Available from: Drug Discov Today [Internet]. 26 (4) (2021) 931–950.
[51] Y.S. Loo, R.J. Bose, J.R. McCarthy, I.D. Mat Azmi, T. Madheswaran, Biomimetic bacterial and viral-based nanovesicles for drug delivery, theranostics, and vaccine applications [cited 2023 Jul 5], Available from: Drug Discov Today [Internet]. 26 (4) (2021) 902–915.